Self-potential signals associated with localized leaks in embankment dams and dikes

A Soueid Ahmed, A. Revil, B. Steck, C. Vergniault, Abderrahim Jardani, G. Vinceslas

Engineering Geology 253 (2019) 229–239

Contents lists available at ScienceDirect

Engineering Geology

journal homepage: www.elsevier.com/locate/enggeo

Self-potential signals associated with localized leaks in embankment dams and dikes

A. Soueid Ahmed[a], A. Revil[a,*], B. Steck[b], C. Vergniault[c], A. Jardani[d], G. Vinceslas[e]

[a] Univ. Grenoble Alpes, Univ. Savoie Mont Blanc, CNRS, IRD, IFSTTAR, ISTerre, 38000 Grenoble, France
[b] EDF R&D, 6 quai Watier, 78400 Chatou, France
[c] EDF DI-TEGG, 905 avenue du Camp de Menthe, 13097 Aix-en-Provence, France
[d] Université de Rouen, M2C, UMR 6143, CNRS, Morphodynamique Continentale et Côtière, Mont Saint Aignan, France
[e] CEREMA Normandie Centre, 10 chemin de la Poudrière, 76121 Le Grand Quevilly, France

ARTICLE INFO

Keywords:
Self-potential
Earth dams
Numerical modelling
Leaks detection

ABSTRACT

The self-potential method can be used to detect and monitor anomalous seepages in dams and embankments. In such a case, an electrical field of electrokinetic nature (i.e., associated with pore water flow) can be measured using a set of non-polarizable electrodes typically located at the ground surface or in some wells. This field can be in turn related to the pattern of groundwater flow. We built an experimental dam to investigate to which extent the self-potential method can help characterizing seepages in dams. We first use the finite element method to simulate the ground water flow in a heterogeneous porous and permeable material by solving the groundwater flow equation. The resulting groundwater flow solution is then used to compute the electrical potential distribution by solving the corresponding elliptic partial differential equation. In a preliminary experiment, we could not measure any self-potential anomaly associated with the infiltration of water in the dam. Our numerical simulations showed that the magnitudes of the self-potential anomalies were controlled by (1) the nature of the flow regime (viscous laminar versus inertial laminar flow regimes) and (2) the presence of insulating Polyvinyl Chloride (PVC) tubes located at the end of the preferential flow channels in the structure of the dam. Thanks to these numerical simulations, we added sand at the entrance of the infiltration area in order to reduce the effects of the PVC tubes and to restrain the flow regime to the viscous laminar flow regime. New experiments allowed for detecting a self-potential anomaly with an amplitude of around −9 mV consistent with that obtained through numerical modelling with a finite element simulator. This comparison was used to test the accuracy of the modelling approach and define the strengths and weaknesses of the self-potential method to determine preferential seepages in earth dam structures.

1. Introduction

The flow of the pore water in a porous material is responsible for generating an electric current known as the streaming current, one of the so-called electrokinetic phenomena (e.g., Helmholtz, 1879). This electric current generates in turn an electrical field and the resulting electrical potential distribution can be passively and remotely recorded using a set of non-polarizable electrodes (e.g., Corwin and Hoover, 1979). The self-potential method (SP) is a passive geophysical method according to which the electrical potential distribution associated with such source electric current density distribution in the ground is recorded and analyzed in terms of ground water flow properties. From a historical point of view, the physics behind this electrokinetic self-potential phenomenon has been established long time ago (e.g., Quincke, 1859; von Smoluchowski, 1903) in the viscous laminar flow regime. Sill (1983) was the first to introduce the so-called source current approach to numerically model (with a finite difference approach) the self-potential signals for a variety of geophysical and engineering applications.

The self-potential method is nowadays extensively used in engineering and in environmental geosciences. For instance, it can be used to map aquifer properties (e.g., Ozaki et al., 2014; Soueid Ahmed et al., 2014, 2016a, 2016b), to delineate coal seam fires (e.g., Karaoulis et al., 2014; Revil et al., 2013; Shao et al., 2016; Soueid Ahmed et al., 2018), for tracking contaminated groundwater (e.g., Abbas et al., 2017; Martínez-Pagán et al., 2010; Naudet et al., 2003), fracking (Mahardika

* Corresponding author.
E-mail addresses: abdellahi.soueid-ahmed@univ-smb.fr (A. Soueid Ahmed), andre.revil@univ-smb.fr (A. Revil), barthelemy.steck@edf.fr (B. Steck), christophe.vergniault@edf.fr (C. Vergniault), abderrahim.jardani@univ-rouen.fr (A. Jardani), Gratien.Vinceslas@cerema.fr (G. Vinceslas).

https://doi.org/10.1016/j.enggeo.2019.03.019
Received 7 January 2019; Received in revised form 23 March 2019; Accepted 26 March 2019
Available online 29 March 2019
0013-7952/

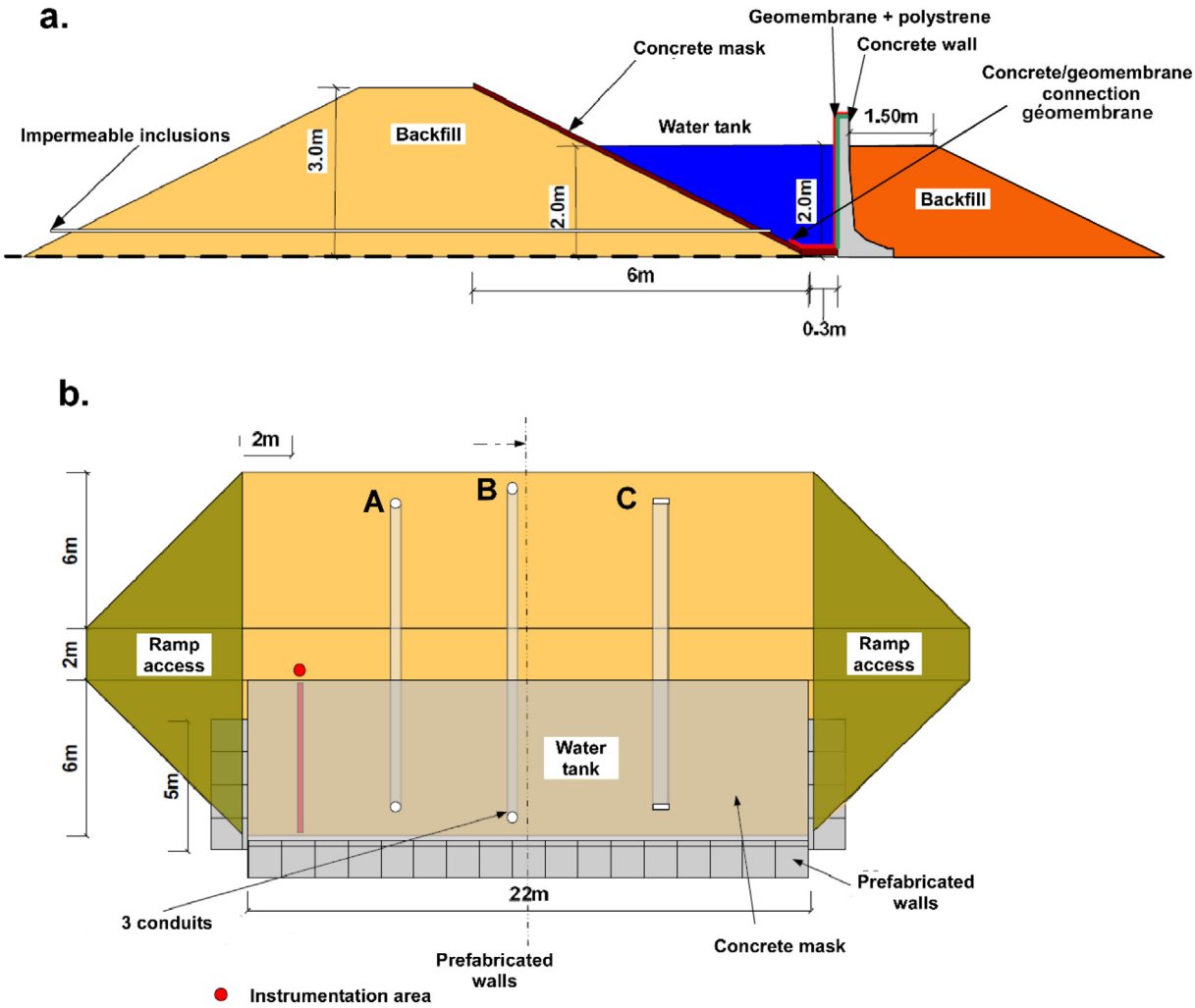

Fig. 1. Sketch of the geometry of the dam. a. Vertical view of the dam. b. View from above the dam. The dam is connected to a water tank that is made by assembling some prefabricated walls. Three high permeability conduits (denoted A, B and C on the figure) are inserted across the core of the dam. This allows for creating preferential flow paths for the water contained in the water reservoir. A concrete mask is put on the downstream part of the core to make it impermeable.

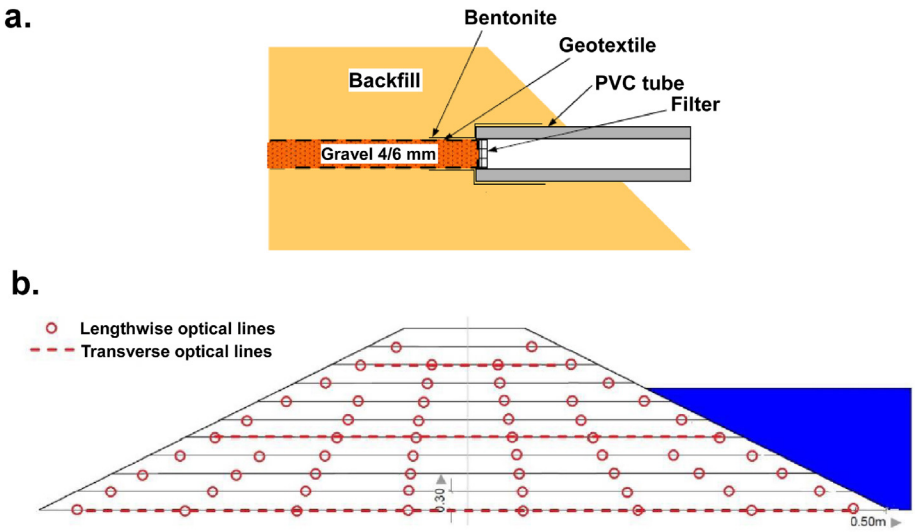

Fig. 2. Design of the dam. a. PVC tubes. b. Optical fiber. The conduit is filled with a 4–6 mm grain size diameter gravel. PVC tubes are used to make impermeable inclusions at the end of each conduit. The optical fiber is used to record the temperature and deformation at several discrete locations through the core of the dam.

Table 1
Distribution of the material properties used for performing the numerical simulations. The quantities K and σ denote the hydraulic conductivity and electrical conductivity, respectively.

	Core	Conduits	Tank	PVC tube	Sand bag
K ($m\,s^{-1}$)	3×10^{-7}	0.4	1	0	2×10^{-2}
σ ($S\,m^{-1}$)	0.008	1.3×10^{-2}	3.7×10^{-2}	10^{-8}	0.0067

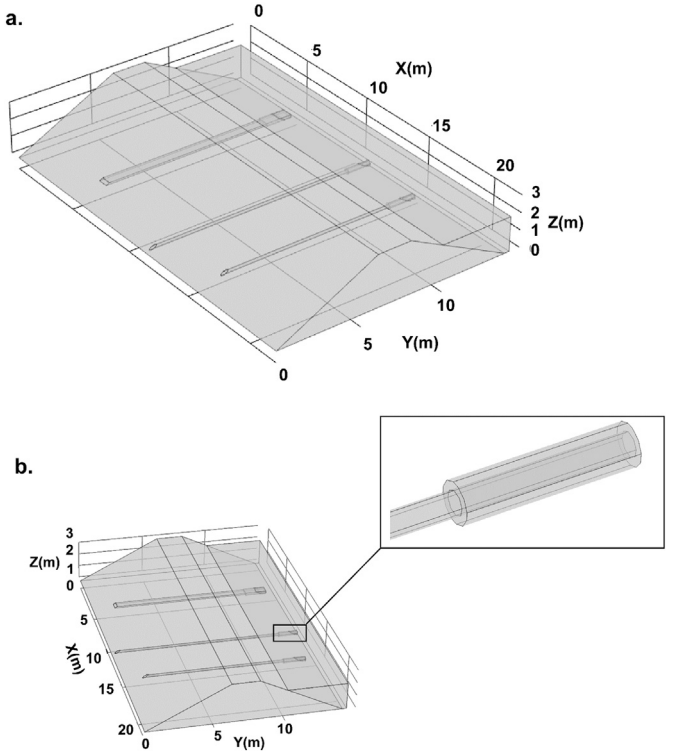

Fig. 3. Simulation domain. a. 3D domain used in the numerical model. b. 3D domain including the PVC tubes. Each component of the dam is modeled as a geometrical subdomain that has specific properties. The PVC tubes are added by surrounding the ends of the conduits with impermeable and electrically resistive subdomains.

et al., 2012; Haas et al., 2013), for geothermal exploration (e.g., Corwin and Hoover, 1979; Hermans et al., 2014), and for a variety of geotechnical applications such as the detection of flow patterns in sinkholes (e.g., Ward, 1990; Jardani et al., 2007a,b,c), landslides (Colangelo et al., 2006), dams (Al-Saigh et al., 1994) and vadose zone hydrogeology (e.g. Aubert et al., 2000; Titov et al., 2002). Since the self-potential method is a passive technique, it is more prone to different sources of noise as extensively discussed in Revil et al. (2012).

Unintended seepage paths in earth dams are caused by backward erosion phenomena and can present a serious threat to their integrity (e.g., Fell et al., 1992, 2003). They may even ultimately lead to their collapse. Therefore, the detection, delineation and continuous monitoring of such seepages in embankments and dams is of paramount importance in any adequate and appropriate maintenance task (Himi et al., 2018; Martínez-Moreno et al., 2018). In this regard, the self-potential method appears as a suitable geoelectrical method for efficiently detecting and delineating seepage paths in embankments and dams. The suitability of the self-potential method for tracking leakages is motivated by several reasons: (i) The high sensitivity of this method to the flow of groundwater. (ii) The easiness of setting up a self-potential survey and (iii) the low financial cost of the required equipment. A recent review regarding the use of self-potential signals as a non-intrusive groundwater flow sensors can be found in Revil et al. (2017).

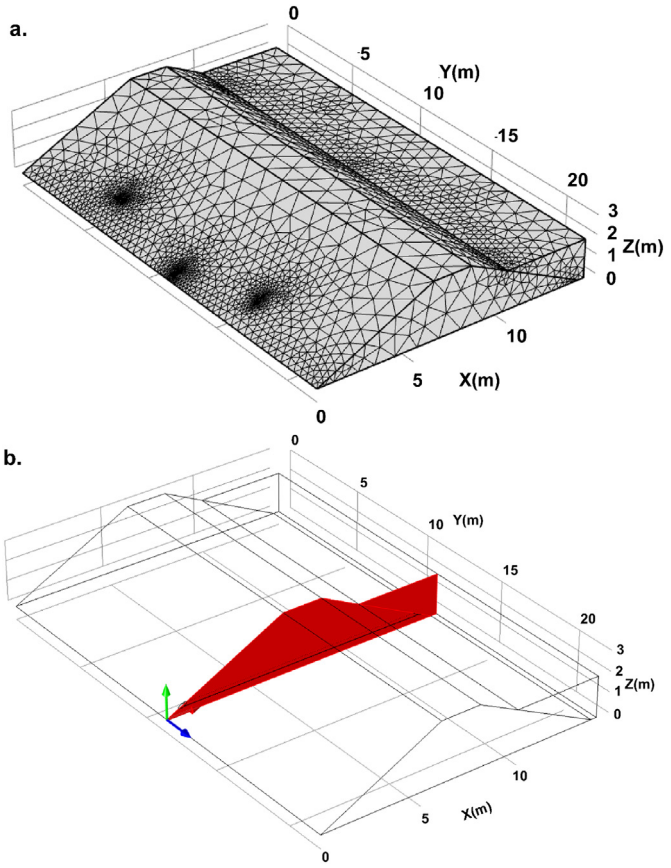

Fig. 4. The mesh and the cross-section used to plot the result. a. Finite element mesh used for solving the equations. A total of 187,371 tetrahedral elements and 24,583 triangular elements are used to mesh the system. We use second order finite elements for solving the partial differential equations. b. Plane going through the central conduit (conduit B) used to show the 2D distribution of the potential in the flow direction.

Various works have been reported in the literature regarding the use of self-potential signals to localize seepages in earth dams. For instance, Panthulu et al. (2001) employed the self-potential method to detect and depict seepage areas in two saddle dams in Rajasthan, India. Their self-potential signals revealed negative anomalies that were in accordance with the localization of independent seepage measurements performed on the same dams. Sheffer and Oldenburg (2007) developed a finite volume code for modelling the self-potential responses associated to the fluid flow in porous media. They interpreted the self-potential response associated to the seepage through an earth embankment in British Columbia, Canada. Bolève et al. (2007, 2009) studied the influence of the Reynolds and Dukhlin numbers on the self-potential signals of electrokinetic nature. They investigated the self-potential anomalies when the intensity of seepage through an embankment is modified. Moore et al. (2011) performed self-potential measurements in order to investigate potential seepage through a moraine dam in California. They concluded that the moraine dam was not suffering from erosion seepage. They attributed the negative self-potential anomalies they recorded to gravitational groundwater flow in the shallow subsurface and in a fault conduit.

Any successful self-potential study that will lead to a comprehensive characterization of potential pathways for seepages and a cost-effective anti-leaking policy for embankments maintenance will probably need the use of numerical modelling techniques. Such numerical models should be able to accurately predict the self-potential distribution across the embankment and therefore help understanding and characterizing the flow across it and allow for better interpretation of the

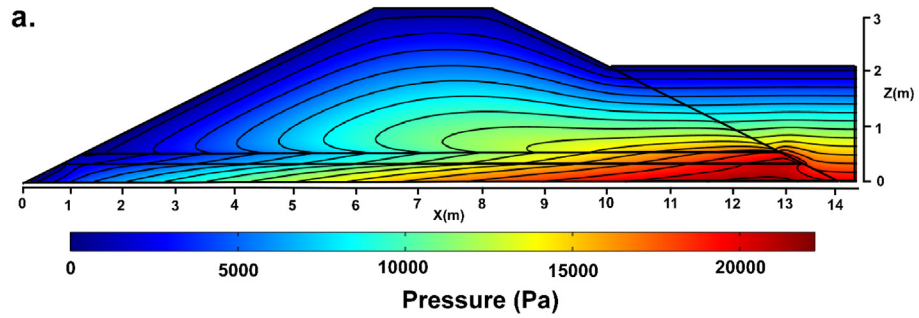

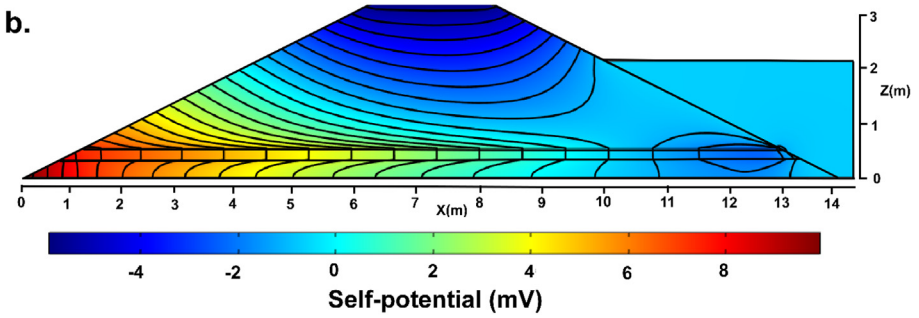

Fig. 5. Pressure and self-potential distributions. a. Pressure distribution in the conduit B. We notice that the pressure is maximum at the entrance of the infiltration area. b. Self-potential distribution for simulations without taking into account the effect of the Reynolds number and without modelling the PVC tubes. The black lines denote the contours of the self-potential distribution.

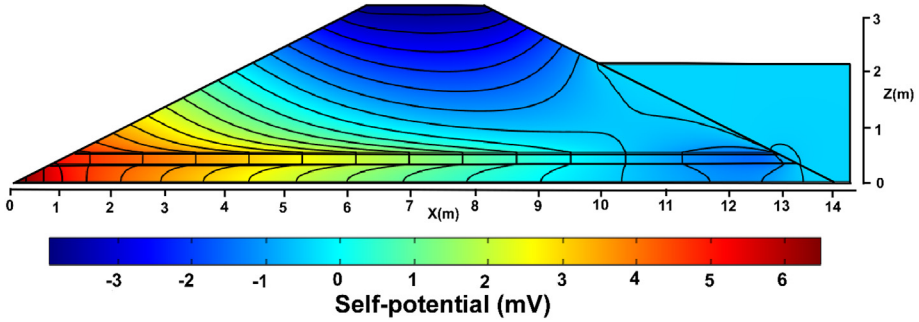

Fig. 6. Self-potential distribution for simulations without the PVC tubes and with the Reynolds number. The effect of the Reynolds number (*Re*) is to reduce the amplitude of the self-potential anomaly by a factor of $1 + Re \approx 2.5$ (in this case). High Reynolds number are therefore implying weak amplitudes of the self-potential anomalies.

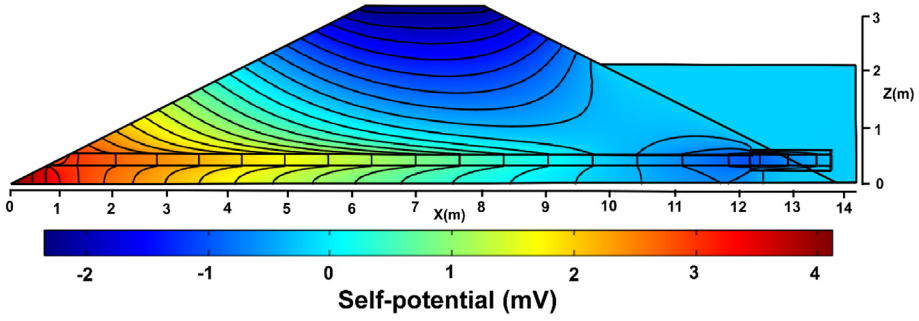

Fig. 7. Self-potential distribution for simulations with the PVC tubes and the Reynolds number effect. Cumulating the effect of the PVC tubes to the Reynolds number ones drastically reduces the amplitude of the self –potential anomaly recorded at the entrance of infiltration area. The self-potential anomaly drops to -0.4 mV, which is likely below the sensitivity of the self-potential acquisition system and cannot be recorded in the field.

collected self-potential data. In addition, these numerical tools could be used to assess the usefulness of the self-potential method on a given embankment prior to performing any self-potential survey.

In this paper, we work on an experimental earth dam that was built by EDF (Electricité de France) in collaboration with CEREMA (Centre d'Etudes et d'Expertise sur les Risques de l'Environnement, la Mobilité et l'Aménagement). The dam is connected to a water tank and contains three high permeability conduits that allow water passage through its core. The goal of this experiment is to study under which conditions the self-potential method is able to detect the presence of the seepage areas in the dam and to identify which factors (such as material types and flow regime) can play a role in the quality of the acquired self-potential data. In addition, the well-known structure of the dam makes it easier to validate numerical models. In parallel, we implemented a 3D numerical scheme that mimics the behavior of this experimental dam. It is based on coupling the groundwater flow equation to the generated electric potential of electrokinetic nature. By doing so, we can predict the self-potential response of the dam and therefore perform a sensitivity study on different parameters such as: the materials used for building the dam, the salinity of the water contained in the tank, the size of the conduits. Despite all prior investigations, the effect of the flow regime has not been investigated in details in the literature and is undertaken in this work.

Our numerical tool is general and can be adapted to any embankment or earth dam if the user provides the geometry and material composition of the structures, in terms of hydraulic and electrical properties. As the self-potential method is widely used for detection of leaks in embankments and dams, we believe that our numerical tool

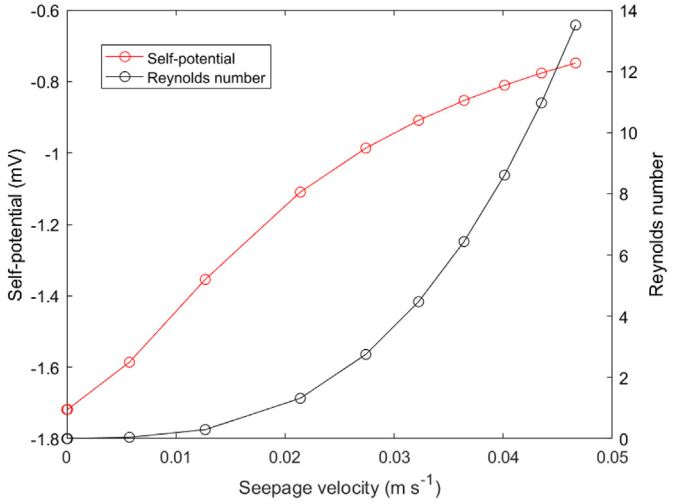

Fig. 8. Evolution of the self-potential anomaly at the entrance of the infiltration area of the conduit B and the Reynolds number with material grains size in the conduit B. The self-potential anomaly is given with respect to the seepage (Darcy) velocity **u**. It is recorded at the entrance of the conduit B. The augmentation of the Reynolds number decreases the amplitude of the self-potential anomaly. In our case, the grains size of the gravel that the conduit B is filled with vary between 4 mm and 6 mm which gives a Reynolds number that is around 2.5.

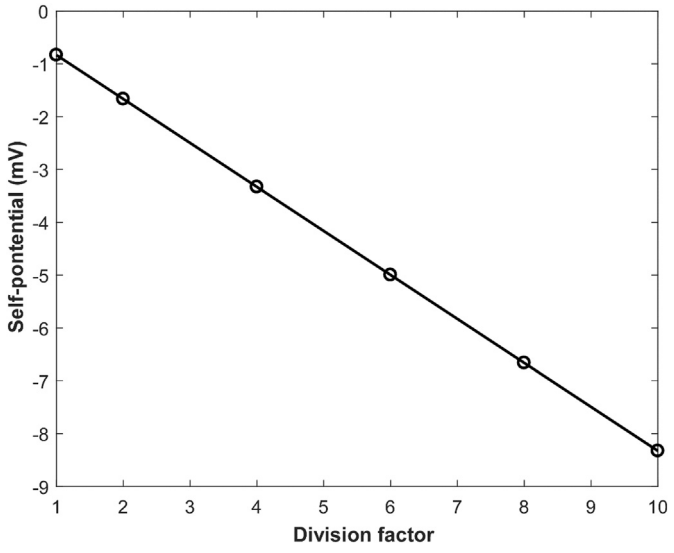

Fig. 9. Change in the self-potential anomaly at the entrance of the conduit B, with the respect to the electric conductivity of the whole structure including the core of the dam, the conduits, and the water of the reservoir. The division factor represents the number by which we divide the conductivity of the structure to make it more resistive.

will be of major importance in helping engineers performing survey designs and knowing even prior to going to the field if they will be able to detect and record any self-potential anomaly related to a given seepage velocity.

2. Theoretical background

The streaming potential signals are generated by the flow of water in porous media and more precisely by the drag of the excess of electrical charges contained in the diffuse layer coating the grains. Therefore, the self-potential signal is expected to depend on the nature of the regime flow, namely the viscous laminar versus inertial laminar flow regimes. In this section, we present the underlying physics in both

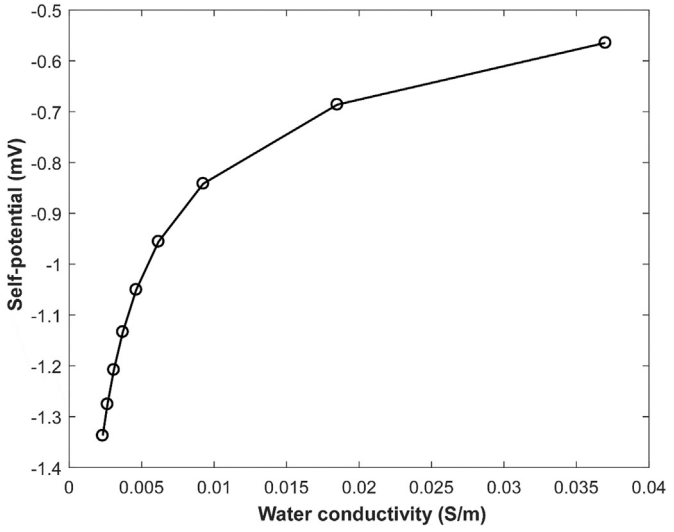

Fig. 10. Change in the self-potential anomaly with the respect to change of electrical conductivity of the water in the reservoir. This case aims to explore the influence of the salinity of the water of the reservoir on the amplitudes of the self-potential anomalies. We notice that the more conductive the water, the weaker the self-potential anomaly. This suggests that the presence of fresh water improves the amplitude of the measured self-potential signals.

flow regimes. These flow regimes can be characterized based on the values of the so-called Reynolds number *Re* (Reynolds, 1883). For small values of the Reynolds number($Re \leq 1$), the flow regime is considered to be viscous laminar, and for Reynolds number comprised between 1 and up to 100), the flow regime is called inertial laminar flow regime (Teng and Zhao, 2000).

When working in the inertial flow regime, the effect of the Reynolds number must be taken into account. According to Bolève et al. (2007), the Reynolds number *Re* is given by,

$$Re = \frac{1}{2}(\sqrt{1 + c} - 1) \tag{1}$$

where c is defined by

$$c = \frac{\beta \rho^2 g}{\eta^2} \frac{d_0^2}{F(F-1)} \nabla h \tag{2}$$

where ∇h is the hydraulic head gradient (dimensionless), d_0(m) is the size of the grains, F (dimensionless) is the formation factor (a power law function of porosity ϕ with $F = \phi^{-m}$, where m is typically in the range 1.5 to 2.5), g denotes the acceleration of the gravity field, ρ and η are the mass density (kg m^{-3}) and dynamic viscosity of water (in Pa s), respectively, and $\beta = 0.00225$ (Bolève et al., 2007).

Under the inertial laminar flow regime, the Reynolds number is taken into account through an apparent hydraulic conductivity K (in m s^{-1}), given by

$$K = \frac{K_0}{1 + Re} \tag{3}$$

where K_0 is the hydraulic conductivity (in m s^{-1}) under the viscous laminar regime and is given for a granular medium with grain diameter d_0 by (Revil and Cathles, 1999)

$$K_0 = \frac{d_0^2 \rho g}{24 F^3 \eta} \tag{4}$$

On the other hand, in an isotropic fully water-saturated heterogeneous medium, the fluid flow can be described under steady-state conditions by the groundwater flow equation, given by:

$$-\nabla \cdot \left(\frac{K}{\rho g} \nabla p \right) = Q_s \tag{5}$$

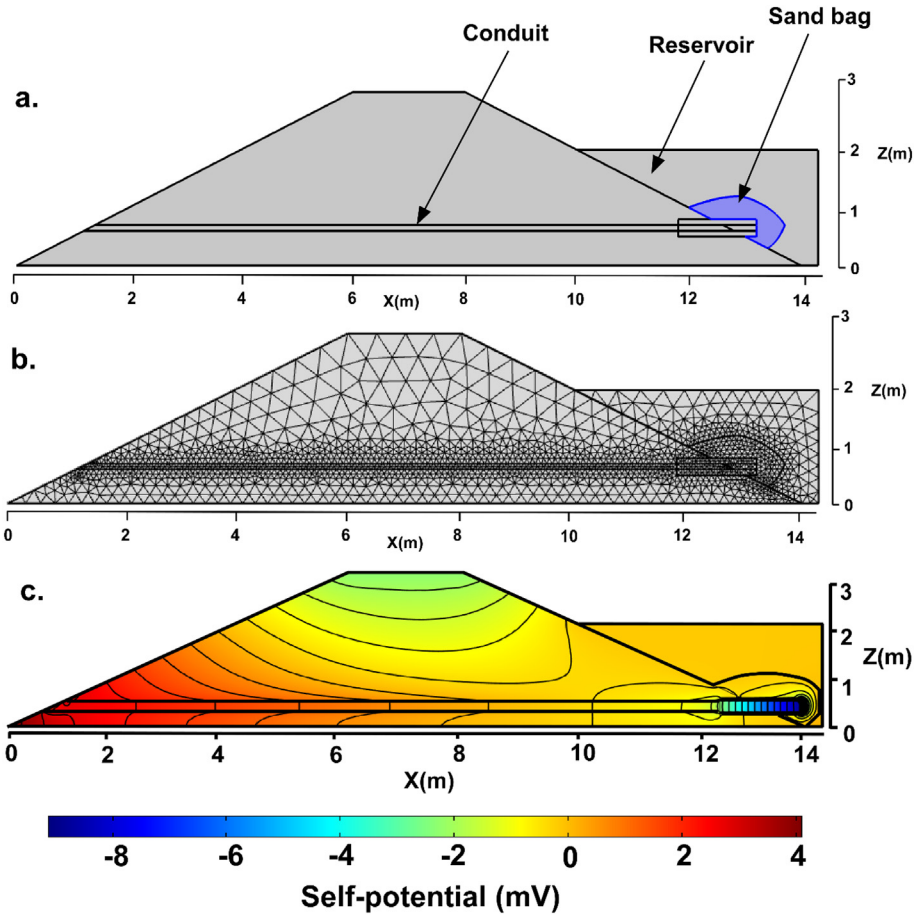

Fig. 11. Numerical modelling of modification of the dam. a. Vertical view of the dam. b. Finite element mesh. c. Self-potential distribution after adding a porous material is added at the entrance of the conduit. The blue domain models the porous material added to the entrance of the conduit B. This figure shows how the modification of the dam was modeled. The porous material placed at the entrance of the area of infiltration was modeled as a new subdomain (blue domain) which is meshed and identified through each hydraulic and electric conductivities. The self-potential anomaly is relatively strong (approximately −9 mV with respect to the crest) but very localized in the vicinity of the inflow area. (For interpretation of the references to colour in this figure legend, the reader is referred to the web version of this article.)

where p (in Pa) is the pore water pressure, Q_s (s^{-1}) is a source term that represents any external fluid flow sources. Eq. (6) is solved with the following boundary conditions:

$$p = p_0 \quad \text{on} \quad \Gamma_D \tag{6}$$

$$-\hat{\mathbf{n}}\cdot K\nabla p = 0 \quad \text{on} \quad \Gamma_N \tag{7}$$

where Γ_D and Γ_N denote the Dirichlet's and Neumann's boundaries, respectively, $\hat{\mathbf{n}}$ denotes the outward unit vector that is normal to Γ_N, and p_0 denotes a prescribed pressure value imposed along the boundary Γ_D. Once Eq. (6) has been solved, we can compute the fluid flow (seepage) velocity $\mathbf{u}$, which is given by the Darcy's law

$$\mathbf{u} = -\frac{K}{\rho g}\nabla p \tag{8}$$

We now consider the equations that describe the electrical problem. In fact, the total current density $\mathbf{j}$ (Am^{-2}) is given by (Sill, 1983; Jardani et al., 2007a,b,c):

$$\mathbf{j} = -\sigma\nabla\varphi + \widehat{Q}_V\mathbf{u} \tag{9}$$

where σ($S\,m^{-1}$) is the electrical conductivity of the medium, φ is the electrical potential (V), $\widehat{Q}_V$ (C m^{-3}) is the effective excess charge density per unit pore volume. This quantity can be related to the hydraulic conductivity according to (e.g., Jardani et al., 2007a,b,c)

$$\log_{10}\widehat{Q}_V = -3.49 - 0.82\log_{10}K \tag{10}$$

In our approach we neglect the effect of the salinity on the volumetric charge density (see Jougnot et al., 2015, and Guarracino and Jougnot, 2018, for more refined models). The continuity equation for electrical charges states that

$$\nabla\cdot\mathbf{j} = 0 \tag{11}$$

which implies from Eqs. (9) and (11) that the potential φ is solution of the following elliptic differential equation

$$\nabla\cdot(\sigma\nabla\varphi) = \nabla\cdot(\widehat{Q}_V\mathbf{u}) \tag{12}$$

Eq. (12) is solved numerically with the following boundary conditions:

$$\varphi = 0 \quad \text{on} \quad \Gamma = \Gamma_D \tag{13}$$

$$-\hat{\mathbf{n}}\cdot[\sigma\nabla\varphi - \widehat{Q}_v\mathbf{u}] = 0 \quad \text{on} \quad \Gamma = \Gamma_N \tag{14}$$

where $\hat{\mathbf{n}}$ is the outward unitary vector that is normal to Γ_N.

3. Experimental design

EDF and the CEREMA designed an experimental earth dam that has the following dimensions: length of 22 m, 14 m of width, 3 m of height and a slope of 1/2. A geomembrane and drainage sealing device is disposed at the interface between the foundation soil and the structure. The dam is connected to a water tank. Several precast concrete walls were assembled together to close the tank. A polypropylene geomembrane was put on the walls of the tank in order to make them waterproof. A 15 cm concrete layer was deposited on the slope of the structure to avoid possible erosion caused by the water tank and to be representative of the commonly used embankments claddings. Fig. 1 illustrates the geometry of the dam and the reservoir tank as well as their dimensions.

Three conduits were designed to go through the core of the dam as shown in Fig. 1. They are used to simulate fluid pathways inside the embankment and the presence of seepage areas of known shapes and dimensions. Two of the conduits have a diameter of 0.2 m and the third one has a 0.6 m × 0.1 m rectangular shape. One of the conduits is

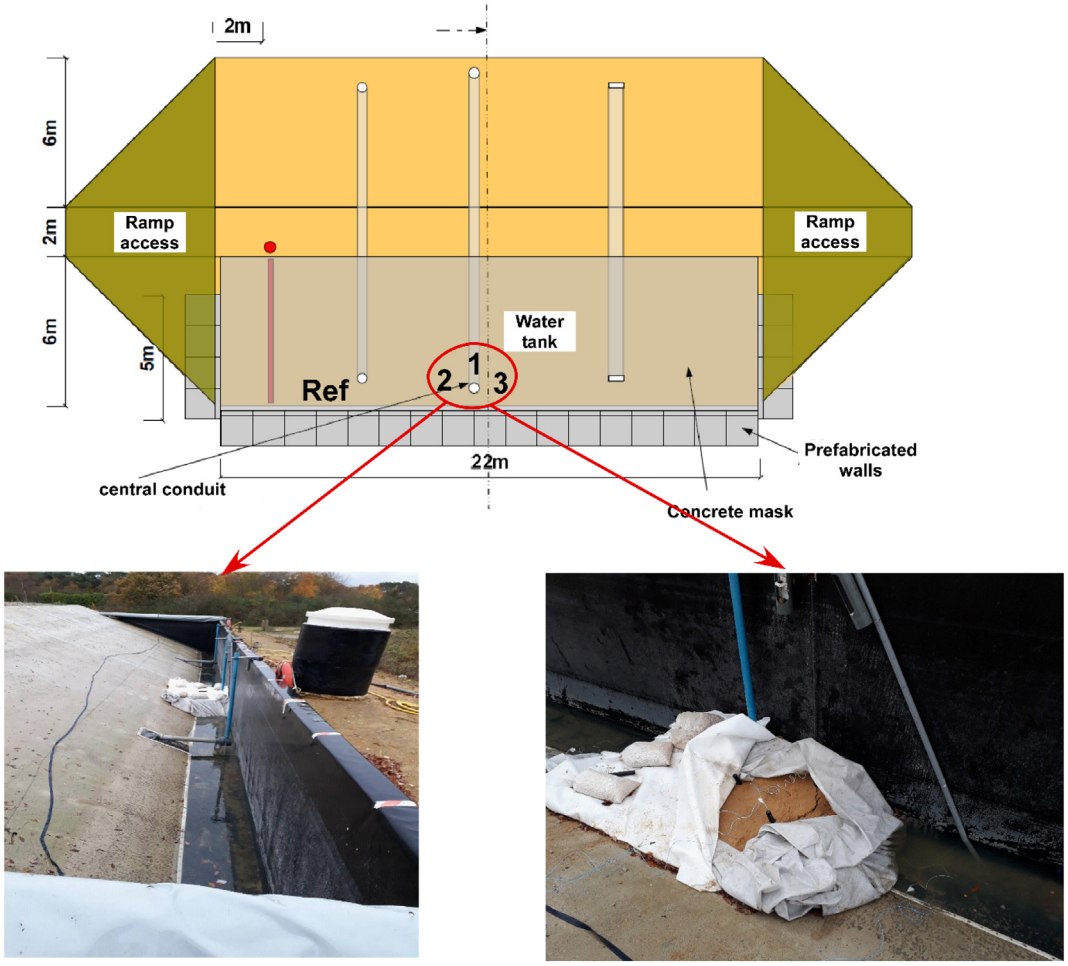

Fig. 12. Representation of the proposed modification of the dam. Three electrodes numbered 1, 2 and 3 are located on the top of the sand. The reference electrode is placed in the tank and is denoted by Ref on the figure. The lower left image shows a side view of the tank while the lower right image shows a view of the sand bag and the electrodes.

located at 2.7 m from the top of the dike and the other one is located 2.1 m from it.

The conduits are filled with gravel (4 mm - 6 mm grain diameter) to mimic high permeability preferential paths for the water across the core of the dam. However, we mention that for the sake of the present study, only the parallelepiped conduits are used (i.e, conduits A and B). The ends of each conduit are performed with PVC sleeves (see Fig. 2a). This is done to allow for installing opening and closure valves at the end of the conduit that it is connected to the tank and also to be able to use any device (such as a pressure transducer) for measuring the leakage rate on the end that is on the other side of the dam. The core of the dam is built by superimposing seven layers of backfill materials whose properties are described in Table 1. Tensiometric probes are put inside the core of the dam to measure the hydraulic potential of the soil. In addition, TDR water content probes are added to the aforementioned instrumentation system. The water tank is maintained during the experiments at a level of 2 m. All the water that flows through the conduits is reintroduced in the tank reservoir using a pump equipped with a non-return valve. Furthermore, a weather station has been installed near the dam to collect the data related to the environment. It is composed of a temperature sensor, a relative moisture sensor, a rain gauge, a pyranometer, and a sonic anemometer.

4. Numerical investigation

Our goal here is to create a numerical model that will allow us understanding and interpreting the self-potential signatures recorded on the dam during groundwater flow in the differential flow regimes and using a variety of boundary conditions. This model will give us the possibility to perform a sensitivity analysis to see which factors can influence the electrical potential distribution in dams. The numerical model consists in solving the semi-coupled equations defined in Section 2. Such partial differential equations can be solved using the finite element method. For that purpose, we use the commercial software Comsol Multiphysics 5.3, which is a partial differential equation solver.

As a first step, the geometry of the simulation must be assembled. We built the 3D geometry of the simulation domain by combining several subdomains corresponding (1) to the core of the dam, (2) the three conduits, (3) the PVC tubes, as well as (4) the reservoir. In fact, we model our dam to have three conduits through which the water contained in the reservoir can go through. This aims to mimic the presence of seepage areas through the core of the dam. It is not necessary to physically model the tank per se, as this can be done through appropriate boundary conditions. Nevertheless, since it may be interesting to represent the electrical potential contours inside the tank to know the extent of the propagation of the electrical potential across the domain of simulation, we decided to physically model the tank and to assign to it the properties of the water that it contains. Fig. 3 shows the geometry of the simulation domain. This geometry is the same as the one of the experimental dam, that is: 3 m of height, 22 m long, 14 m depth. It is connected to a 2 m level water tank. The geometry and the design of the experimental dam are described in more details in Section

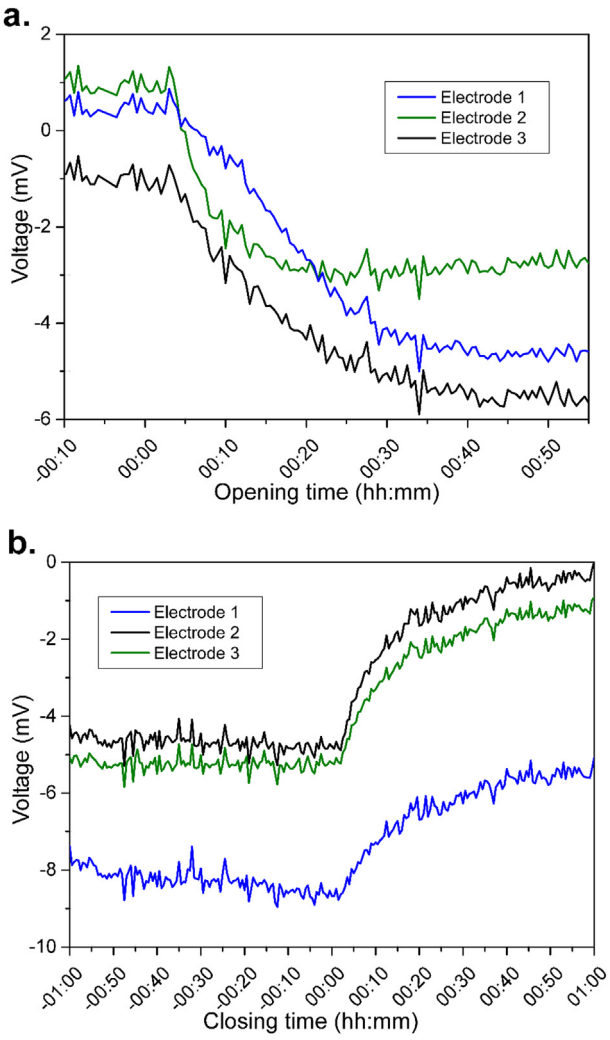

Fig. 13. Self-potential signals recorded at the electrode placed on top of the sand bag. a. The time series show the built-up of the self-potential anomaly when the leakage is initiated. b. This time series show the relaxation of the self-potential anomaly when the leakage is stopped. The time series are not corrected for drifting.

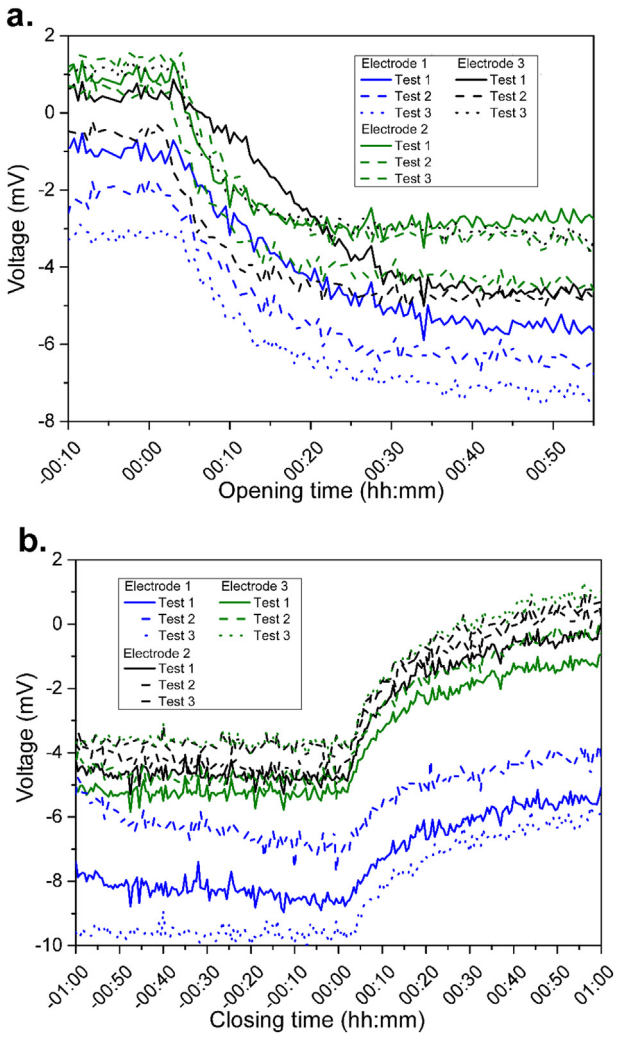

Fig. 14. Reproducibility of the self-potential data. a. The time series show the built-up of the self-potential anomaly when the leakage is initiated. b. This time series show the relaxation of the self-potential anomaly when the leakage is stopped. The time series are not corrected for drifting. We performed three experiences (Test 1, Test 2, and Test 3) in which we activated and deactivated the leakage three times. This was done to make sure that the self-potential data measured in the sand bag are reproducible.

3.

Once the geometry assembly has been achieved, we need to discretize the different subdomains. We use unstructured tetrahedral elements for performing the finite element mesh and quadratic or second order finite elements for solving the equations. The finite element mesh is represented in Fig. 4a. Next, we present several test cases that show how the self-potential signals change within different modelling scenarios.

4.1. Simulations in the laminar flow regime

As a first simulation, we will run our model without taking into account the effects of the Reynolds number, i.e. we consider that we are working under viscous laminar flow regime conditions. We also neglect the presence of the PVC tubes i.e., we did not geometrically create the subdomains corresponding to them. The aim of this simulation is to have a reference model that can be used for comparison of different simulation scenarios.

A critical point in the modelling is about the choice of the boundary conditions that will be applied. For the hydraulic problem, we impose the pressure of the reservoir at the boundary corresponding to the entrance of the conduits, then we impose no pressure flux boundary conditions at the bottom of the dam as well as the walls of the of the tank. Atmospheric pressure boundary condition is applied to the remaining boundaries. For the electrical potential problem, insulation boundary conditions are applied to all the external boundaries of the simulation domain while continuity flux boundary conditions are applied to internal boundaries. We consider that the steady state has been reached. Since in our experiment, only the central conduit (conduit B) was used as a preferential pathway for the water flow and thus for generating the self-potential anomaly, we will only consider this conduit for visualizing our simulation results. In particular, we use the 2D plane shown in Fig. 4b to plot the results.

Fig. 5a shows the fluid pressure distribution across the conduit B after opening the valves that generate the water flow. The maximum pressure is reached at the entrance of the conduit. Once the fluid pressure distribution has been computed, the self-potential distribution can be obtained by solving the electrical potential equation whose source term depends on the pressure. From a didactic point of view, it is more meaningful to represent the contours of the self-potential distribution. To do so, we choose the cut plane shown in Fig. 4b. The self-potential distribution along this plane is illustrated in Fig. 5b. This self-

potential distribution exhibits a negative anomaly of around −2 mV at the seepage area inlet.

4.2. Simulations accounting for the Reynolds number

We will now take into account the effect of the Reynolds number in our simulations. In this case, we are working under the inertial laminar flow regime conditions. We computed the Reynolds number in the three conduits and we found that it is approximately equal to 1.5. The Reynolds number inside the core of the dam is expected to be too small as the fluid flow does not occur in this area and therefore its Reynolds number can be neglected. Fig. 6 shows the self-potential distribution along with electrical equipotentials when the Reynolds number is accounted for.

The numerical model shows that at the entrance of the seepage area, the negative self-potential anomaly is −0.8 mV. This is in accordance with the equations presented in Section 2 which state that the effect of the Reynolds number is to reduce the self-potential signal amplitude by a factor of $1 + Re$, which corresponds in our case to around 2.5 ($1 + Re \approx 2.5$). This numerical experience showed the importance of taking into account the Reynolds number in order to accurately interpret the measured self-potential data. Indeed if the fluid flow enters into the inertial flow regime, the measured self-potential signal will be significantly decreased especially if the electrodes are located far from the self-potential current sources. We will come back later on regarding the dependence between the self-potential signal and the nature of the fluid flow regime.

4.3. Simulations with PVC tubes

The PVC tubes were used to make the open ends of the conduits. We would like to numerically investigate the effect of these tubes on the self-potential distribution in the dam and the tank. This will give us insights on the potential responsibility of these tubes in the low quality self-potential signal that we recorded during the seepage experiment before performing the modification of the dam. The PVC tubes are modeled as subdomains that are impermeable to fluid flow and electrically insulating (see Table 1).

Fig. 7 shows the self-potential distribution obtained when taking into account the PVC tubes in our simulations. One can notice that the self-potential signal has become quite weak, the anomaly amplitude at the entrance of the infiltration area drops now to around - 0.4 mV. This makes the presence of the PVC tubes suspicious and the low quality measured signal can be partially attributed to the presence of these tubes. However, we still notice that the self-potential distribution does not radically change from the previous one when the PVC tubes were not modeled. In other words, the PVC tubes weakened the self-potential signal but did not lead to the presence of unphysical anomalies that cannot be interpreted. Their presence combined with the effect of the Reynolds number can make the self-potential signal too weak to a level that it becomes undetectable with the self-potential recording system.

4.4. Sensitivity analysis

We investigate now the effect of changing the size of the grains of the conduits and the electrical properties of the core of the dam as well as the water of the tank on the self-potential signal. We performed a series of numerical experiments. First, we look at the influence of the permeability of the conduits on the amplitude of the self-potential anomaly generated in the seepage areas. The order of magnitudes of the permeability is changed by switching the size of the gravel grains in the conduits.

Each grain size is associated to a different Reynolds number under the assumption that the pressure gradient is unchanged. In fact, only the Reynolds number is a physical parameter that must be taken into account for each dam that is subject to seepages while the PVC tubes are specific to the design of the experiment. It can be neglected in the current sensitivity analysis in which we aim to portray general results about the self-potential signatures measured on dams. Thus, these simulations are performed without taking into account the effect of the PVC tubes. We point out that for these simulations, the hydraulic head is maintained constant, i.e., the pressure head gradient is constant. Fig. 8 shows the evolution of the amplitude of the self-potential anomaly with the Reynolds number and the seepage velocity at the entrance of the infiltration area. The increase of the value of the Reynolds number is associated with a decrease of the amplitude of the self-potential anomaly.

In our case, the Reynolds number is around 1.5 then the measured anomaly is expected to be around −1 mV. We can learn from this experience that the Reynolds number has large influence on the self-potential distribution and it can significantly decreases its amplitude. On the other hand, it is known that the intensity of the self-potential anomalies depends on the electrical properties of the medium in which the fluid flow occurs. Conductive media are expected to retain the electric current and to reduce the amplitude of the measured self-potential anomalies. We perform a sensitivity analysis on the electrical conductivity of the dam including the water tank. For different values of this electrical conductivity we measure the self-potential anomaly at the entrance of the central conduit (conduit B). This experience is however hypothetical and is infeasible in practice. It is performed only to make sure that the numerical model behave adequately as expected and does reproduce the expected physical phenomena. Fig. 9 shows the results of this experience. The amplitude of the self-potential signal measured at the entrance of the conduit B increases with respect to the global electrical resistivity of the dam. This is in complete accordance with the Ohm's law and it means that the conduction processes increase as well.

We now consider the influence of the electrical conductivity of the water used to fill the tank. We assume here that the salinity does not affect the volumetric charge density (see Ikard et al., 2012, for an extensive discussion of this topic). That said, more refined models can be used if needed (Guarracino and Jougnot, 2018). This conductivity is changed and the corresponding amplitude of the self-potential anomaly at the entrance of the conduit B is recorded. Fig. 10 illustrates the results of such experience. The self-potential anomaly decreases when the water becomes more conductive. This suggests that using fresh water for the tank can help increasing the amplitude of the measured self-potential anomalies.

5. Experimental and numerical results

Experimental measurements were performed with the use of Petiau non-polarizable electrodes and with a 20 channels Keysight 34980A acquisition station (https://www.keysight.com). All measurements are made in a monitoring mode with a fixed base station used as a reference. The SP signals were recorded during a variable duration ranging from 1 h to 24 h using a time step of 30 s. Furthermore, an electrical resistivity tomography profile has been performed at the crest of the dam, which allowed us to estimate the electrical resistivity of the core of the dam to be around 120 Ohm m. Using the configuration described in Section 3, the recorded self-potential signals did not show any variation when the flow was activated and the self-potential anomalies were covered by the noise level which is 1 mV for this kind of acquisition systems. This low self-potential anomaly motivated the use of a numerical simulation to understand these observations. Indeed our previous simulations (see Section 4) identified two reasons for the low magnitude of the self-potential signals (1) the presence of the PVC tubes and (2) the occurrence of inertial flow, which is reflected by the relatively high value of the Reynolds number.

In order to counteract the presence of the PVC tubes and the occurrence of the inertial flow regime, we propose to modify the inflow experiment of the dam by adding a porous material (sand) at the

entrance of the conduit B. Adding a sand bag at the entrance of the inflow area is expected to address these two issues and make the experiment closer to real field conditions. The sand used for the experiment is characterized by grain diameters in the range 0.1 mm to 4 mm in order to be quite permeable but at the same time keeping the flow in the viscous laminar flow regime. The methodology that we are following consists in two steps. In the first step, we numerically validated the feasibility and usefulness of adding a porous material at the inlet of the infiltration area. Then, in a second step and depending on the results of the simulations, we performed this change in the experimental design of the dam to observe the change on the measured self-potential signals.

Fig. 11a and b display a vertical view of the simulation domain taking into account the modification of the dam. We use our numerical modelling tool to construct a simulation of the flow and its associated self-potential signals accounting for the effect of the bag of sand placed at the entrance of the inflow area. Fig. 11c demonstrates that the simulated self-potential anomaly in the vicinity of the seepage reaches now a magnitude close to −9 mV. We also notice that the potential lines are concentrated around the seepage area and inside the bag. Therefore, in order to observe such self-potential anomaly, the electrodes should be placed in this area. It is now clear, at least numerically that the proposed modification of the dam, can clearly improve the quality of the signal potential signal measured in the vicinity of the porous material (i.e. the sand bag). These encouraging simulation results spurred us on conducting the construction of the proposed modification on the experimental dam.

Therefore, a physical experiment was performed to check if adding the sand can generate a self-potential anomaly with an amplitude similar to the predicted signals. Self-potential measurements were made with 3 Petiau electrodes (e.g., Petiau and Dupis, 1980; Petiau, 2000) placed at the surface of the sand body (see Fig. 12). This type of electrode was chosen because of its high stability and weak dependence on temperature. The reference electrode was placed inside the water tank far from the leakage area. This reference electrode was used to address the issue of variations of water temperature. Fig. 13 shows the self-potential signals measured on the three electrodes placed in the sand bag. We can observe that when the system reaches its equilibrium state, negative self-potential anomalies reaching −4 to −5 mV are recorded. This is consistent with the range of the self-potential anomalies predicted by the numerical model. An anomaly of around −8 mV is even measured on electrode 1, which is the closest to the leak. In order to further validate the modification of the dam that we did, we performed several activation and deactivation of the leakage in different days and we measured the self-potential anomalies on the same electrodes. Fig. 14 shows the results of such experiment. As one can see, the self-potential anomalies are perfectly reproducible.

6. Conclusion

We have developed a numerical approach for modelling the self-potential anomalies generated by seepages in earth dams included saturated and unsaturated conditions. Our model is used to diagnose the reasons for the absence or presence of self-potential anomalies associated with water infiltration in an experimental dam. When the dam was first designed, we were unable to observe any self-potential signal associated with the inflow of water through the preferential flow paths crossing the core of the dam. This observation motivated the implementation of a numerical approach to simulate the behavior of the self-potential signals associated with the flow of the ground water in the dam and to understand the reasons behind the low magnitude of the recorded self-potential signals. Our simulations have shown that the relatively high Reynolds numbers and the presence of PVC tubes in the structure were the main reasons behind these observations. In the second set of experiments, a bag of sand was placed at the entrance of the conduits in order to change the fluid flow regime (from laminar inertial to laminar viscous) and therefore to reduce the influence of the Reynolds number. In addition, the presence of a porous material at the entrance of the preferential flow path was more realistic with respect to natural conditions Applying this configuration to the dam significantly improved the quality of the recorded self-potential data and allowed for generating detectable anomalies at the vicinity of the seepage area. The present work shows the importance of performing numerical modelling prior to any self-potential survey on dams and dikes to check if the configuration of the considered dam allows for the measurement of detectable self-potential anomalies. In addition, numerical modelling gives the possibility for optimizing the design of the self-potential survey by choosing the optimal positions of the electrodes.

Acknowledgments

This work was supported by Electricité De France (EDF). The postdoc of Abdellahi Soueid Ahmed is funded by EDF through a grant with the CNRS. We thank the two referees for their very constructive reviews of this manuscript.

References

Abbas, M., Jardani, A., Ahmed, A.S., Revil, A., Brigaud, L., Bégassat, P., Dupont, J.P., 2017. Redox potential distribution of an organic-rich contaminated site obtained by the inversion of self-potential data. J. Hydrol. 554, 111–127.

Al-Saigh, H.N., Mohammed, S.Z., Dahham, S.M., 1994. Detection of water leakage from dams by self-potential method. Eng. Geol. 37 (2), 115–151. https://doi.org/10.1016/0013-7952(94)90046-9.

Aubert, M., Dana, I.N., Gourgaud, A., 2000. Internal structure of the Merapi summit from self-potential measurements. J. Volcanol. Geotherm. Res. 100, 337–343.

Bolève, A., Crespy, A., Revil, A., Janod, F., Mattiuzzo, J.L., 2007. Streaming potentials of granular media: influence of the Dukhin and Reynolds numbers. J. Geophys. Res. 112 (B8).

Bolève, A., Revil, A., Janod, F., Mattiuzzo, J.L., Fry, J.J., 2009. Preferential fluid flow pathways in embankment dams imaged by self-potential tomography. Near Surf. Geophys. 7 (5–6), 447–462.

Colangelo, G., Lapenna, V., Perrone, A., Piscitelli, S., Telesca, L., 2006. 2D self-potential tomographies for studying groundwater flows in the Varco d'Izzo landslide (Basilicata, southern Italy). Eng. Geol. 88 (3–4), 274–286. https://doi.org/10.1016/j.enggeo.2006.09.014.

Corwin, R.F., Hoover, D.B., 1979. The self-potential method in geothermal exploration. Geophysics 44 (2), 226–245.

Fell, R., MacGregor, P., Stapledon, D., 1992. Geotechnical Engineering of Embankment Dams. Balkema, Rotterdam (ISBN 9054101288).

Fell, R., Wan, C.F., Cyganiewicz, J., Foster, M., 2003. Time for development of internal erosion and piping in embankment dams. J. Geotech. Geoenviron. 127, 307–314.

Guarracino, L., Jougnot, D., 2018. A physically based analytical model to describe effective excess charge for streaming potential generation in water saturated porous media. J. Geophys. Res. 123 (1), 52–65.

Haas, A.K., Revil, A., Karaoulis, M., Frash, L., Hampton, J., Gutierrez, M., Mooney, M., 2013. Electrical potential source localization reveals a borehole leak during hydraulic fracturing. Geophysics 78 (2), D93–D113. https://doi.org/10.1190/GEO2012-0388.1.

Helmholtz, H., 1879. Study concerning electrical boundary layers. Weidemann Ann. Phys. Chem. 7, 337–382.

Hermans, T., Nguyen, F., Robert, T., Revil, A., 2014. Geophysical methods for monitoring temperature changes in shallow low enthalpy geothermal systems. Energies 7 (8), 5083–5118. https://doi.org/10.3390/en7085083.

Himi, M., Casado, I., Sendros, A., LoveraaL, R., Rivero, L., Casasa, A., 2018. Assessing preferential seepage and monitoring mortar injection through an earthen dam settled over a gypsiferous substrate using combined geophysical methods. Eng. Geol. 246, 212–221. https://doi.org/10.1016/j.enggeo.2018.10.002.

Ikard, S.J., Revil, A., Jardani, A., Woodruff, W.F., Parekh, M., Mooney, M., 2012. Saline pulse test monitoring with the self-potential method to nonintrusively determine the velocity of the pore water in leaking areas of earth dams and embankments. Water Resour. Res. 48https://doi.org/10.1029/2010WR010247. W04201.

Jardani, A., Revil, A., Boleve, A., Crespy, A., Dupont, J.P., Barrash, W., Malama, B., 2007a. Tomography of the Darcy velocity from self-potential measurements. Geophys. Res. Lett. 34 (24), L24403. https://doi.org/10.1029/2007GL031907.

Jardani, A., Revil, A., Bolève, A., Crespy, A., Dupont, J.-P., Barrash, W., Malama, B., 2007b. Tomography of the Darcy velocity from self-potential measurements. Geophys. Res. Lett. 34, L24403. https://doi.org/10.1029/2007GL031907.

Jardani, A., Revil, A. Bolève, Crespy, A., Dupont, J.-P., Barrash, W., Malama, B., 2007c. Tomography of the Darcy velocity from selfpotential measurements. Geophys. Res. Lett. 34, L24403. https://doi.org/10.1029/2007GL031907.

Jougnot, D., Linde, N., Haarder, E.B., Looms, M.C., 2015. Monitoring of saline tracer movement with vertically distributed self-potential measurements at the HOBE agricultural test site, Voulund, Denmark. J. Hydrol. 521, 314–327.

Karaoulis, M., Revil, A., Mao, D., 2014. Localization of a coal seam fire using combined

self-potential and resistivity data. Int. J. Coal Geol. 128, 109–118. https://doi.org/10.1016/j.coal.2014.04.011.
Mahardika, H., Revil, A., Jardani, A., 2012. Waveform joint inversion of seismograms and electrograms for moment tensor characterization of fracking events. Geophysics 77 (5), ID23–ID39. https://doi.org/10.1190/GEO2012-0019.1.
Martínez-Moreno, F.J., Delgado-Ramos, F., Galindo-Zaldívar, J., Martín-Rosales, W., López-Chicano, M., González-Castillo, L., 2018. Identification of leakage and potential areas for internal erosion combining ERT and IP techniques at the Negratín Dam left abutment (Granada, southern Spain). Eng. Geol. 240, 74–80. https://doi.org/10.1016/j.enggeo.2018.04.012.
Martínez-Pagán, P., Jardani, A., Revil, A., Haas, A., 2010. Self-potential monitoring of a salt plume. Geophysics 75 (4), WA17-WA25.
Moore, J.R., Boleve, A., Sanders, J.W., Glaser, S.D., 2011. Self-potential investigation of moraine dam seepage. J. Appl. Geophys. 74 (4), 277–286.
Naudet, V., Revil, A., Bottero, J.-Y., Bégassat, P., 2003. Relationship between self-potential and redox conditions in contaminated groundwater. Geophys. Res. Lett. 30 (21), 2091. https://doi.org/10.1029/2003GL018096.
Ozaki, Y., Mikada, H., Goto, T.N., Takekawa, J., 2014. Simultaneous inversion of self-potential for estimating hydraulic parameters and streaming current coefficient. In: The 18th International Symposium on Recent Advances in Exploration Geophysics (RAEG 2014).
Panthulu, T.V., Krishnaiah, C., Shirke, J.M., 2001. Detection of seepage paths in earth dams using self-potential and electrical resistivity methods. Eng. Geol. 59 (3–4), 281–295. https://doi.org/10.1016/S0013-7952(00)00082-X.
Petiau, G., 2000. Second generation of lead-lead chloride electrodes for geophysical applications. Pure Appl. Geophys. (3), 357–382.
Petiau, G., Dupis, A., 1980. Noise, temperature coefficient and long time stability of electrodes for telluric observations. Geophys. Prospect. 28 (5), 792–804.
Quincke, G., 1859. Concerning a new type of electrical current. Annalen der Physik 107 (2), 1.
Revil, A., Cathles, L.M., 1999. Permeability of shaly sands. Water Resour. Res. 35 (3), 651–662.
Revil, A., Karaoulis, M., Johnson, T., Kemna, A., 2012. Review: some low-frequency electrical methods for subsurface characterization and monitoring in hydrogeology. Hydrogeol. J. 20 (4), 617–658. https://doi.org/10.1007/s10040-011-0819-x.
Revil, A., Karaoulis, M., Srivastava, S., Byrdina, S., 2013. Thermoelectric self-potential and resistivity data localize the burning front of underground coal fires. Geophysics 78 (5), B259–B273.
Revil, A., Ahmed, Soueid A., Jardani, A., 2017. Self-potential: a non-intrusive ground water flow sensor. J. Environ. Eng. Geophys. 22 (3), 235–247. https://doi.org/10.2113/JEEG22.3.235.
Reynolds, O., 1883. An experimental investigation of the circumstances which determine whether the motion of water shall he direct or sinuous, and of the law of resistance in parallel channels. Philos. Trans. R. Soc. Lond. 174, 935–982.
Shao, Z., Revil, A., Mao, D., Wang, D., 2016. Induced polarization signature of coal seam fires. Geophys. J. Int. 208 (3), 1313–1331.
Sheffer, M.R., Oldenburg, D.W., 2007. Three-dimensional modelling of streaming potential. Geophys. J. Int. 169 (3), 839–848.
Sill, W.R., 1983. Self-potential modeling from primary flows. Geophysics 48, 76–86.
von Smoluchowski, M., 1903. Contribution à la théorie de l'endosmose électrique et de quelques phénomènes corrélatifs. Bull. Int. Acad. Sci. Cracovie 8, 182–200.
Soueid Ahmed, A., Jardani, A., Revil, A., Dupont, J.P., 2014. Hydraulic conductivity field characterization from the joint inversion of hydraulic heads and self-potential data. Water Resour. Res. 50 (4), 3502–3522. https://doi.org/10.1002/2013WR014645.
Soueid Ahmed, A., Jardani, A., Revil, A., Dupont, J.P., 2016a. Specific storage and hydraulic conductivity tomography through the joint inversion of hydraulic heads and self-potential data. Adv. Water Resour. 89, 80–90. https://doi.org/10.1016/j.advwatres.2016.01.006.
Soueid Ahmed, A., Jardani, A., Revil, A., Dupont, J.P., 2016b. Joint inversion of hydraulic head and self-potential data associated with harmonic pumping tests. Water Resour. Res. 52 (9), 6769–6791. https://doi.org/10.1002/2016WR019058.
Soueid Ahmed, A., Revil, A., Jardani, A., Chen, R., 2018. 3D geostatistical inversion of induced polarization data and its application to coal seam fires. Geophysics 83 (3), E133–E150. https://doi.org/10.1190/GEO2017-0232.1.
Teng, H., Zhao, T.S., 2000. An extension of Darcy's law to non-Stokes flow in porous media. Chem. Eng. Sci. 55, 2727–2735.
Titov, K., Ilyin, Y., Konosavski, P., Levitski, A., 2002. Electrokinetic spontaneous polarization in porous media: petrophysics and numerical modelling. J. Hydrol. 267, 207–216.
Ward, S.H., 1990. Geotechnical and Environmental Geophysics. Vol. 1. Society of Exploration Geophysicists, Tulsa, Oklahoma, pp. 147–190.